iScience

CellPress
OPEN ACCESS

Article

ABHD12 contributes to tumorigenesis and sorafenib resistance by preventing ferroptosis in hepatocellular carcinoma

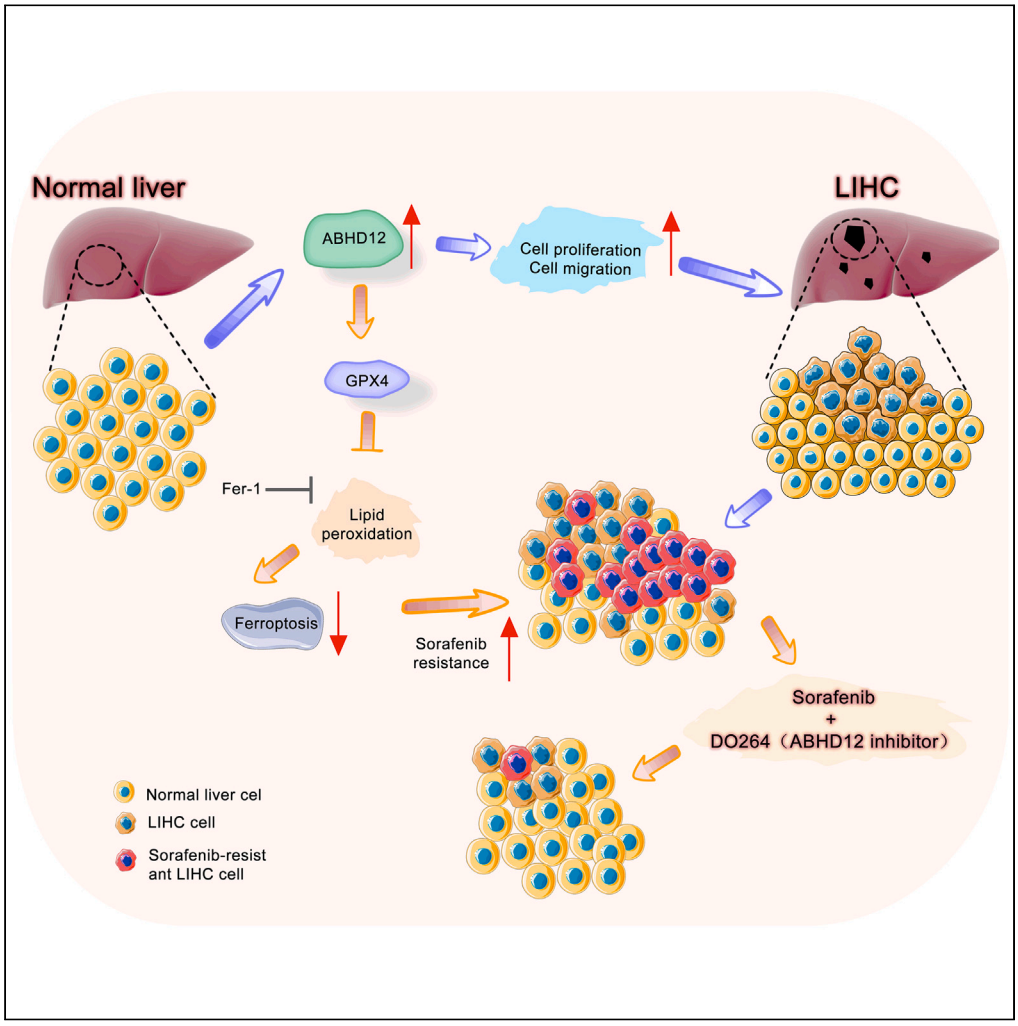

Mengxing Cai, Jingwen Luo, Chunxiu Yang, Xiaopeng Yang, Cheng Zhang, Lixin Ma, Yibin Cheng

zhangcheng1988@whu.edu.cn (C.Z.)
malixing@hubu.edu.cn (L.M.)
chengyibin@hubu.edu.cn (Y.C.)

Highlights

ABHD12 is a promising potential biomarker in the diagnosis and prognosis of LIHC

ABHD12 contributes to tumorigenesis in LIHC

Biological alterations of ABHD12 regulates sorafenib resistance by ferroptosis

Co-delivery of sorafenib and DO264 represents a novel therapeutic strategy for LIHC

Cai et al., iScience *26*, 108340
December 15, 2023
https://doi.org/10.1016/j.isci.2023.108340

iScience

CellPress
OPEN ACCESS

Article

ABHD12 contributes to tumorigenesis and sorafenib resistance by preventing ferroptosis in hepatocellular carcinoma

Mengxing Cai,[1,3] Jingwen Luo,[1,3] Chunxiu Yang,[2] Xiaopeng Yang,[1] Cheng Zhang,[1,*] Lixin Ma,[1,*] and Yibin Cheng[1,4,*]

SUMMARY

Sorafenib induces ferroptosis, making it a useful treatment against advanced liver hepatocellular carcinoma (LIHC). However, sorafenib resistance is extremely common among LIHC patients. Here, we used a comprehensive approach to investigate the effects of ABHD12, which regulates tumorigenesis and sorafenib resistance in LIHC. We validated *ABHD12* expression was upregulated in LIHC tissue, which correlated with worse overall survival and related to tumor size or stage. ABHD12 facilitated a pro-tumorigenic phenotype involving increased cell proliferation, migration, and clonogenicity as well as sorafenib resistance. Knockout of *ABHD12* sensitized liver cancer cells to sorafenib-induced ferroptosis. Co-delivery of sorafenib and ABHD12 inhibitor into a nude mouse model enhanced therapeutic efficacy for LIHC. Our study demonstrates that ABHD12 contributes to tumor growth and sorafenib resistance in liver cancer, which indicate the promising potential of *ABHD12* in diagnosis and prognosis as well as highlight the potential therapeutic applications for co-delivery of sorafenib and ABHD12 inhibitor.

INTRODUCTION

Liver hepatocellular carcinoma (LIHC) is the common type of cancer and constitutes a major health concern around the world, due to its high mortality rate.[1–3] Risk factors for LIHC include chronic infection with hepatitis B or hepatitis C virus, exposure to alcohol and aflatoxins, as well as somatic mutations and chromosomal aberrations.[4,5] Although the molecular mechanism of LIHC is not completely clear, early detection of liver cancer can improve the survival rate of LIHC patients by more than 50%.[6,7] However, the majority of LIHC patients are already in intermediate or advanced stages when diagnosed[8]; hence, novel molecular markers for early diagnosis and identification of appropriate therapeutic targets are of great importance for improving patient survival.

Targeted molecular therapy with the multikinase inhibitor sorafenib remains the only approved systemic therapy for advanced LIHC patients for whom surgical resection is no longer an option.[9] Sorafenib prolonged survival of patients with advanced LIHC,[10,11] and it has been approved as a first-line treatment for advanced LIHC.[12] However, a substantial proportion of patients with advanced LIHC become resistant to sorafenib, which worsens prognosis.[13,14] Therefore, delineating the mechanisms underlying resistance of LIHC to sorafenib is of utmost importance.

Sorafenib is a strong inducer of ferroptosis in LIHC cells.[15,16] Ferroptosis is a type of regulated cell death that results from iron-dependent lipid peroxide accumulation, and it differs from apoptosis, necrosis, and autophagy.[17,18] Ferroptosis can be triggered by high extracellular glutamate or small molecules such as sorafenib, erastin, and sulfasalazine that block import of cystine/glutamate.[19] Ferroptosis can be induced by genetic deletion or small-molecule inhibition of the antioxidant enzyme glutathione peroxidase 4 (*GPX4*).[20,21] Ferroptosis may be more selectively induced in cancer cells than in normal cells; thus, inducing ferroptosis selectively in cancer cells may enhance the efficacy of sorafenib against LIHC and thereby bypass or counteract sorafenib resistance.[22–24]

ABHD12 on chromosome 20 (20p11.21) encodes a neutral lipase that acts on monoacylglycerols such as endocannabinoid 2-arachidonoylglycerol.[25] The endocannabinoid system has been reported to be closely associated with cancer[26]: it induces cell death, inhibits cell proliferation, arrests cell cycle, and prevents tumor migration and invasion in different types of cancers.[27,28] Thus, targeting the endocannabinoid system through ABHD12 may be a treatment against breast cancer.[29] ABHD12 is upregulated in breast cancer tissues and enhance tumorgenicity[30]; in human fibrosarcoma cells, pharmacological blockade of ABHD12 enhances ferroptosis-mediated cell death.[31] In addition, genome-wide association study (GWAS) shows that *ABHD12* may be related to abnormal liver function,[32] but no studies have linked ABHD12 to LIHC.

[1]State Key Laboratory of Biocatalysis and Enzyme Engineering, Hubei Key Laboratory of Industrial Biotechnology, Hubei Collaborative Innovation Center for Green Transformation of Bio-Resources, School of Life Sciences, Hubei University, Wuhan 430062, China
[2]Department of Pathology, Union Hospital, Tongji Medical College, Huazhong University of Science and Technology, Wuhan 430022, China
[3]These authors contributed equally
[4]Lead contact
*Correspondence: zhangcheng1988@whu.edu.cn (C.Z.), malixing@hubu.edu.cn (L.M.), chengyibin@hubu.edu.cn (Y.C.)
https://doi.org/10.1016/j.isci.2023.108340

In this study, we took a comprehensive approach to determine the role of ABHD12 in LIHC tumorigenicity and sorafenib resistance. Bioinformatic and patient sample analysis showed *ABHD12* to be upregulated in liver cancer tissue, and we confirmed experimentally that ABHD12 overexpression upregulated GPX4, preventing ferroptosis, inducing sorafenib resistance, and promoting tumor growth. Moreover, co-delivery of ABHD12 inhibitor and sorafenib slowed cancer progression to a greater extent than sorafenib alone in mouse models. Collectively, our findings identify a new link between ABHD12 and tumorigenesis, and they suggest that ABHD12 contributes to sorafenib resistance by preventing ferroptosis in LIHC.

RESULTS

ABHD12 expression level is associated with tumor size or stage and prognosis of LIHC patients

We identified a total of 7,687 differentially expressed genes (DEGs) between LIHC patients and normal controls from the TCGA database with a threshold defined by $|\log_2(\text{fold change})| > 1.5$ and an adjusted p value < 0.05 (Table S1). Of the 23 members of the *ABHD* family,[33] 10 were differentially expressed in 371 LIHC tissues (Figure 1A). Analysis of mutation patterns based on the CBioPortal website showed that a tiny minority of LIHC patients had genetic alterations in *ABHD* genes (Figures 1B and 1C). Additionally, several *ABHD* genes were overexpressed in the following types of carcinomas compared with healthy tissue: cholangiocarcinoma (CHOL), colon adenocarcinoma (COAD), lymphoid neoplasm diffuse large B cell lymphoma (DLBC), acute myeloid leukemia (LAML), and LIHC (Figure 1D). Notably, *ABHD12* was consistently the most upregulated *ABHD* gene in LIHC, with the level in cancer tissue up to 6-fold the level in healthy tissue. These results indicate that members of the *ABHD* family may regulate tumorigenesis.

To evaluate the prognostic value of *ABHD* genes, we performed Kaplan-Meier analysis of overall survival (OS) and disease-free survival (DFS) (Figures 1E and 1F). High expression of *ABHD12* correlated with poor OS (log rank p = 0.01) and DFS (log rank p = 0.016) in LIHC patients. The p value of other ABHD genes was above 0.05 for OS or DFS; therefore, no such correlation was found for both OS and DFS (Figures S1 and S2).

This analysis identified *ABHD12* as a potential prognostic biomarker for LIHC, so we focused on this gene in all further studies. *ABHD12* was expressed at higher levels in LIHC tissue than in healthy tissue based on TCGA datasets (Figure 1G). *ABHD12* was also significantly upregulated in CHOL and DLBC, underscoring its potential activity in tumorigenesis (Figure 1H).

We also investigated associations between *ABHD12* expression and clinicopathological characteristics of LIHC patients (Figure 2; Table S2). ABHD12 protein expression profiling was validated by immunohistochemistry on a tissue microarray containing 58 cancerous samples and 58 paired samples of adjacent non-tumor tissue from the same LIHC patients. Immunohistochemistry showed that ABHD12 was significantly overexpressed in liver cancer tissues compared with adjacent non-tumor tissues in most LIHC patients ($p < 0.001$) (Figures 2A and 2B). More than 80% of LIHC tumor samples showed high ABHD12 expression (Figures 2C). Generally, ABHD12 protein level in LIHC patients was closely related to tumor size and T stage (Table S3), but not to age, sex, or G stage. Quantitative real-time PCR confirmed that *ABHD12* mRNA was significantly overexpressed in 12 LIHC tissues compared with adjacent non-tumor tissues (Figure 2D). These results indicate that *ABHD12* may be a potential diagnostic and prognostic biomarker for liver cancer.

ABHD12 regulates cell cycle, DNA replication, mismatch repair, and ferroptosis in LIHC cells

To understand how *ABHD12* overexpression may affect LIHC tumorigenesis, gene set enrichment analysis was performed on the TCGA dataset. We found high *ABHD12* expression showed enrichment in the following biological pathways: cell cycle, mismatch repair process, DNA replication, base/nucleotide excision repair, spliceosome, RNA polymerase, and pyrimidine metabolism process, whereas there was a negative regulatory relationship between ABHD12 and mismatch repair process (Figures 3A, 3B, and S3). Additionally, the level of *ABHD12* mRNA correlated positively with cell-cycle-related protein CDK1/7 but negatively with proteins involved in mismatch repair such as MLH3 and MSH3 (Figures 3C and 3D). These data indicate that *ABHD12* might participate in the proliferation and somatic mutation of liver cancer cells. Moreover, we noted that low *ABHD12* expression showed enrichment in signaling pathways involving fatty acid metabolism (Figure 3E). Studies have classified that reprograming of lipid metabolism is closely related to the ferroptosis sensitivity,[34] and the level of *ABHD12* mRNA correlated positively with expression of *GPX4*, a negative regulator of ferroptosis, and negatively with p53, a positive regulator of ferroptosis (Figures 3F and 3G). These data indicate that *ABHD12* might influence ferroptosis in liver cancer cells. These results indicate that *ABHD12* might participate in the proliferation, somatic mutation, and ferroptosis of liver cancer cells.

ABHD12 induces a pro-tumorigenic phenotype and sorafenib resistance by preventing ferroptosis in different kinds of liver cancer cell lines

To explore the effect of ABHD12 on the function of cancer cells, we constructed HepG2 and Huh-7 cell lines stably overexpressing *ABHD12* or from which the gene was deleted (Figures 4A and S4A). Overexpression of *ABHD12* significantly enhanced clonogenic capacity (Figures 4B and S4B) and migration (Figures 4C–4E and S4C–S4E) of liver cancer cells, whereas *ABHD12* knockout negated these effects. Overexpression of *ABHD12* also increased cell proliferation, which was suppressed when *ABHD12* was deleted (Figures 4F–4H and S4F–S4H). The results show that ABHD12 can promote the proliferation and migration ability of liver cancer cells.

Both HepG2 and Huh-7 cells overexpressing or lacking *ABHD12* were treated with sorafenib; regardless of sorafenib treatment, GPX4 protein was significantly upregulated in cells overexpressing *ABHD12* but downregulated in cells lacking *ABHD12*. Similarly, treating wild-type cells with the ABHD12 inhibitor DO264 downregulated GPX4 (Figures 5A and S5A). Studies show that the enzymatic activity of ABHD12 can be

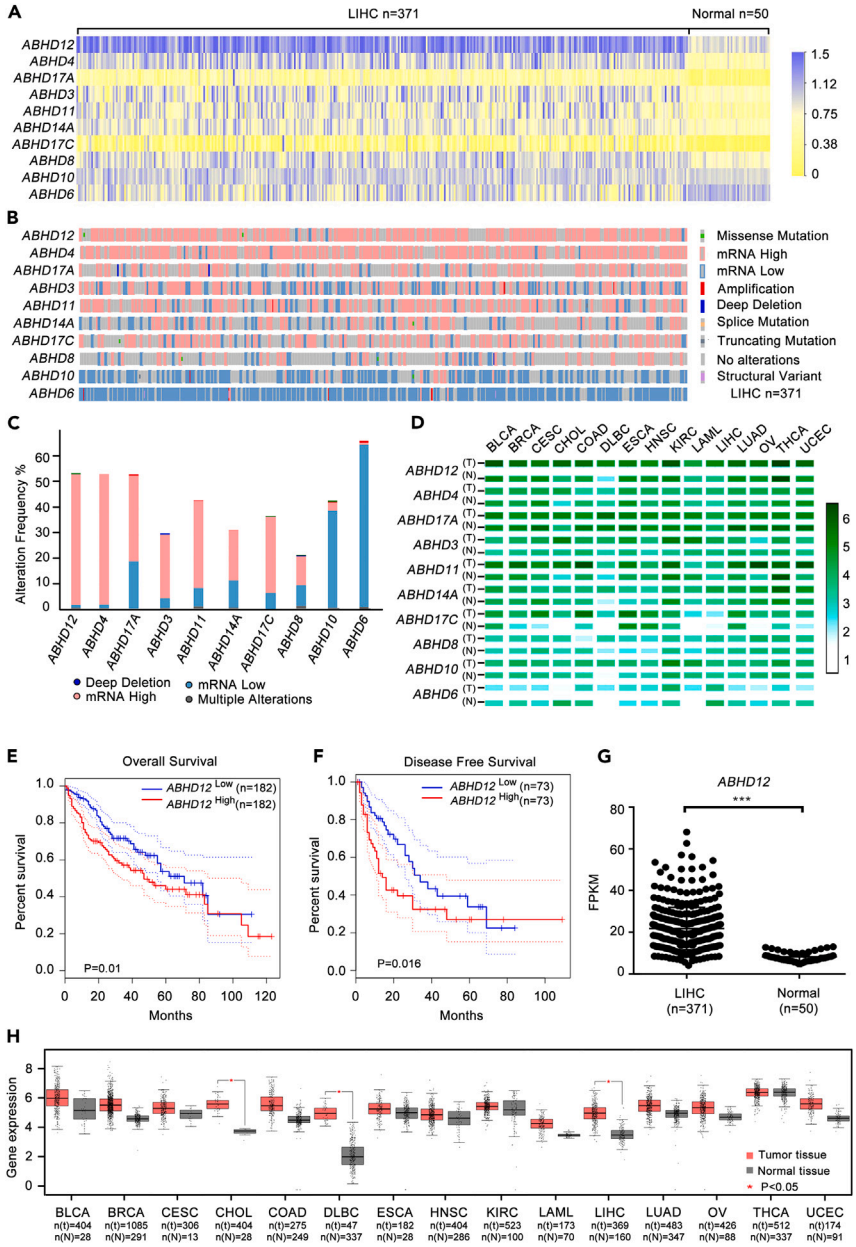

Figure 1. ABHD12 is overexpressed in liver cancer

(A) Heatmap of TCGA samples.

(B) Genetic alterations and expression of *ABHD* genes in LIHC.

(C) Summary of alterations in differentially expressed *ABHD*s in LIHC.

(D) Comparison of *ABHD* expression between various cancers and normal tissue.

(E) Overall survival of LIHC patients, stratified by *ABHD12* expression.

(F) Disease-free survival of LIHC patients, stratified by *ABHD12* expression.

(G) Comparison of *ABHD12* expression between LIHC and normal tissues in the TCGA database. ***$p < 0.001$, unpaired t test.

(H) Fold changes in *ABHD12* gene expression in various cancers. *$p < 0.05$. Abbreviations: *ABHD,* α/β-hydrolase domain-containing; LIHC, liver hepatocellular carcinoma; BLCA, bladder urothelial carcinoma; BRCA, breast invasive carcinoma; CESC, cervical squamous cell carcinoma and endocervical adenocarcinoma; CHOL, cholangiocarcinoma; COAD, colon adenocarcinoma; DLBC, lymphoid neoplasm diffuse large B cell lymphoma; ESCA, esophageal carcinoma; HNSC, head and neck squamous cell carcinoma; KIRC, kidney renal clear cell carcinoma; LAML, acute myeloid leukemia; LUAD, lung adenocarcinoma; OV, ovarian serous cystadenocarcinoma; THCA thyroid carcinoma; UCEC, uterine corpus endometrial carcinoma. N, normal; T, tumor.

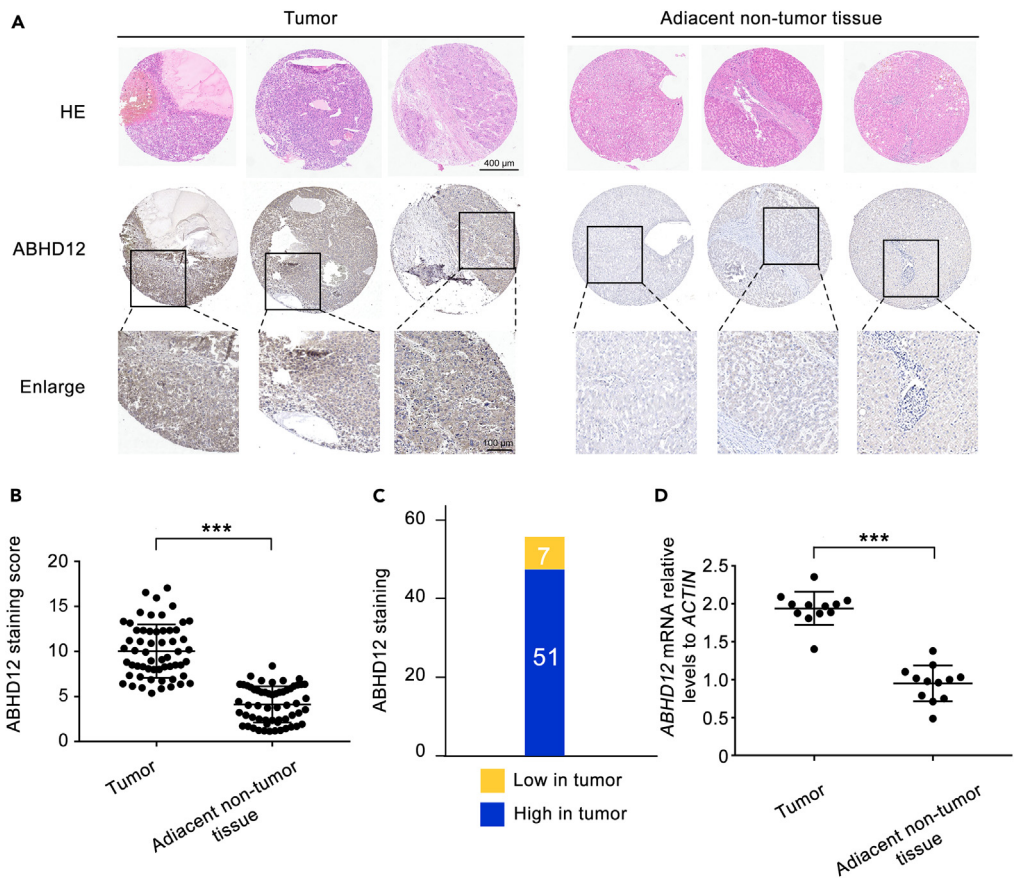

Figure 2. Expression of ABHD12 in liver cancer tissues

Tumor and adjacent non-tumor tissues were taken from LIHC patients, and ABHD12 protein levels were quantified.

(A) Immunohistochemistry of ABHD12 in cancerous and adjacent non-tumor tissues. H&E: scale bar, 400 μm. Enlarged image: scale bar, 100 μm.

(B) Quantitation of ABHD12 expression based on immunohistochemistry (patients, n = 58).

(C) Distribution of ABHD12 levels of 58 patients based on immunohistochemistry.

(D) Quantitative real-time PCR of *ABHD12* mRNA in LIHC tissues and adjacent non-tumor tissues (patients, n = 12). *ACTIN* was used as an internal control. **p < 0.01, ***p < 0.001. Abbreviations: H&E, hematoxylin and eosin staining.

degraded by genetic change of ABHD12 or small-molecule inhibition such as DO264; the results of the present study are consistent with reports in HT1080 fibrosarcoma cells that blockade of ABHD12 potentiates ferroptosis.[31] Given that ferroptosis is driven by intracellular lipid peroxidation, we measured indicators C11-BODIPY$^{581/591}$ of this process.[35] Overexpressing *ABHD12* in HepG2 cells showed fewer lipid peroxidation, regardless of whether sorafenib was present. In contrast, cells lacking *ABHD12* showed greater lipid peroxidation, which sorafenib further increased (Figures 5B and S5B). Ferroptosis also involves the accumulation of reactive oxygen species (ROS).[36] We found that knocking out *ABHD12* or treating cells with ABHD12 inhibitor led to significantly higher ROS than in control cells or cells overexpressing *ABHD12*, regardless of sorafenib treatment (Figures 5C and S5C).

Given that genetic disruption of *ABHD12* sensitizes LIHC cells to ferroptosis, inducing ferroptosis may prevent the emergence of sorafenib resistance.[37] We found that the half-maximal inhibitory concentration (IC_{50}) of sorafenib was 9.68 μM against wild-type cells, 9.37 μM against control cells, 12.08 μM against cells overexpressing *ABHD12*, 7.06 μM against cells lacking *ABHD12*, and 7.93 μM against cells treated with ABHD12 inhibitor, the IC_{50} value of *ABHD12*-OE cells was increased compared with that of the control groups, whereas the IC_{50} value of *ABHD12*-KO groups was decreased (Figure 5D). These results showed that ABHD12 enhanced sorafenib resistance in LIHC. Furthermore, according to the concentration gradient and the corresponding viability index, the drug ZIP synergy scores were calculated, and the results showed that the average and the maximum synergy score were 15.59 and 32.28 in HepG2 cells (Figure 5E). Indeed, treatment with sorafenib and DO264 showed highly synergistic effects in inhibiting tumor proliferation (ZIP synergy scores > 10). We next tested the effect of ABHD12 on the viability of liver cancer cells with sorafenib treatment. As it was talked before in Figure 4F, knockout of *ABHD12* in HepG2 cells reduced viability, whereas overexpression increased it. In the presence of 10 μM sorafenib, cells lacking *ABHD12* showed significantly lower viability than cells overexpressing it (Figure 5F). Similar results were found in Huh-7 cell lines in Figures S5D and S5E.

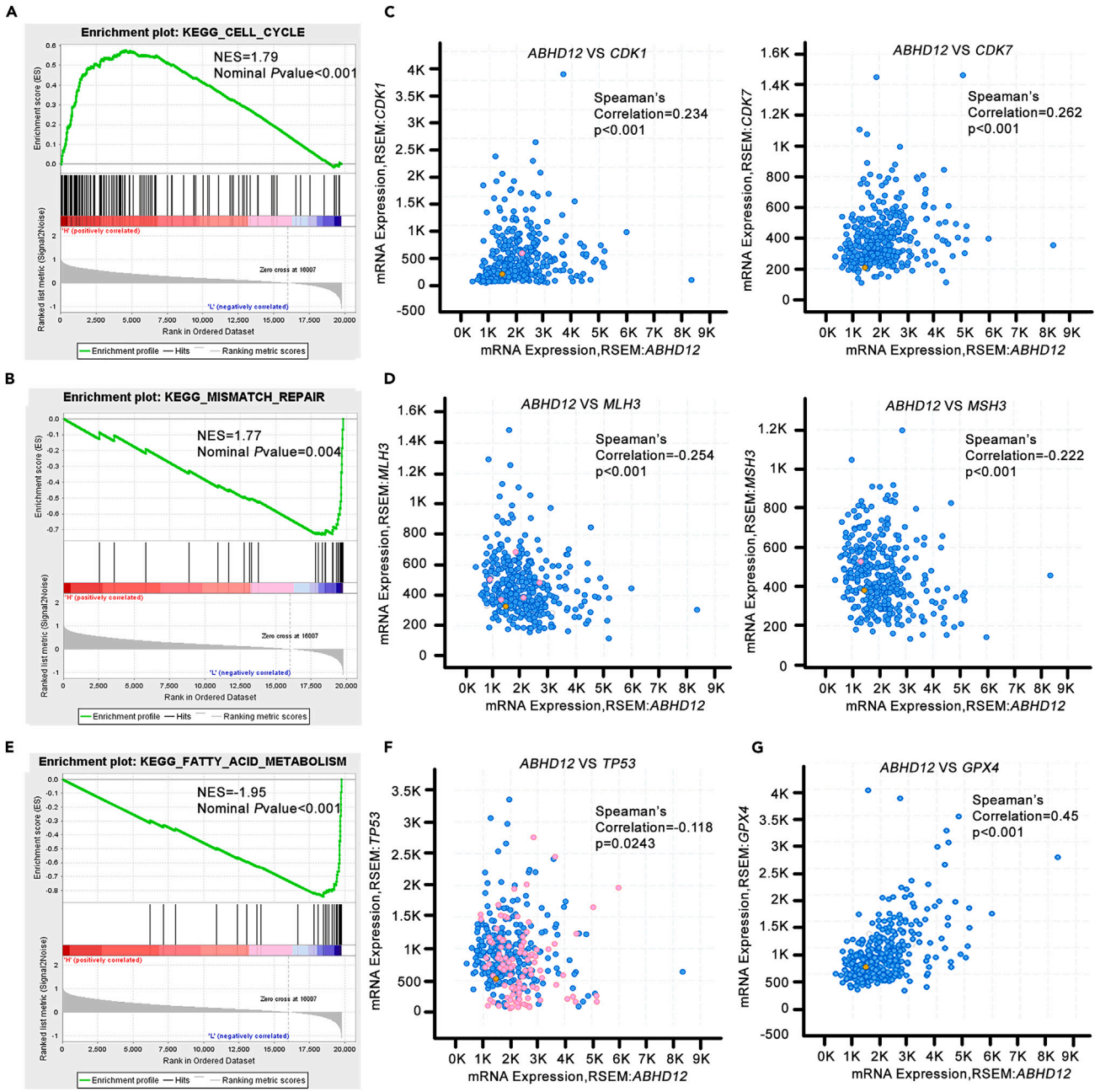

Figure 3. ABHD12 is correlated with different biological processes in LIHC

(A and B) The role of *ABHD12* in biological processes was investigated by gene set enrichment analysis of the TCGA dataset. *ABHD12* expression showed enrichment of genes involved in the cell cycle and mismatch repair.

(C and D) Spearman's correlation analysis identified associations between the level of *ABHD12* mRNA and enrichment of genes in the following biological pathways in LIHC: (C) cell cycle (*CDK1* and *CDK7*); (D) mismatch repair (*MLH3* and *MSH3*).(E) The role of *ABHD12* in biological processes was investigated by gene set enrichment analysis of the TCGA dataset. *ABHD12* expression showed enrichment of genes involved in fatty acid metabolism. (F and G) Spearman's correlation analysis identified associations between the level of *ABHD12* mRNA and enrichment of genes in the following biological pathways in LIHC:

(F) positive regulation of ferroptosis (*p53*);

(G) negative regulation of ferroptosis (*GPX4*). Abbreviations: *CDK1*, cyclin-dependent kinase 1; *CDK7*, cyclin-dependent kinase 7; *MLH3*, mutL homolog 3; *MSH3*, mutS homolog 3; *GPX4*, glutathione peroxidase 4.

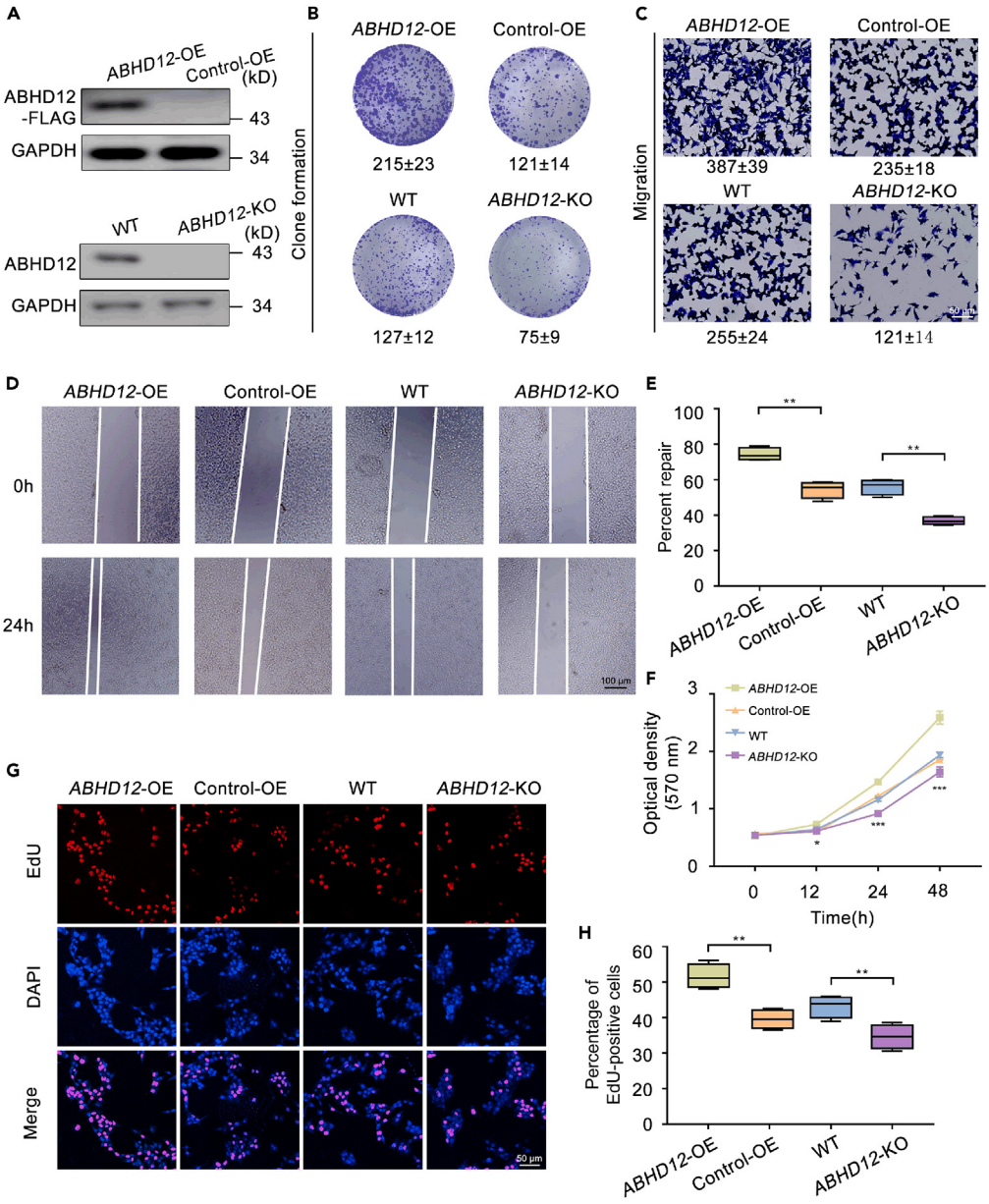

Figure 4. *ABHD12* promotes proliferation and migration of HepG2 cells

Four HepG2 cell lines were used in the following experiments: Control-OE, cells treated with empty viral vector; *ABHD12-OE*, cells overexpressing *ABHD12*; WT, wild-type cells; *ABHD12-KO*, cells from which *ABHD12* was deleted.

(A) Western blot analysis of ABHD12 expression in four HepG2 cell lines; GAPDH was used as an internal control.

(B and C) Representative images and quantification of (B) colony formation assays and (C) migration assays. Scale bar, 50 μm.

(D and E) Representative images of wound healing experiments before and after injury and quantification of migration within 24 h. Scale bar, 100 μm.

(F) Cell proliferation as assessed by MTT assay.

(G and H) Fluorescence micrographs of EdU incorporation into cellular DNA and quantification of EdU^+ cells. Scale bar, 50 μm. All data are presented as the mean ± SD from three independent experiments. *$p < 0.05$, **$p < 0.01$, and ***$p < 0.001$ versus control group. Abbreviations: OE, overexpressing; KO, knock out.

Based on these observations, we hypothesize that ABHD12 promotes sorafenib resistance by detoxifying the intracellular environment during sorafenib-induced ferroptosis. To test this hypothesis, we assessed whether the ferroptosis inhibitor ferrostatin-1 could prevent sorafenib-induced cell death in the absence of *ABHD12*. Indeed, in the presence of sorafenib, this inhibitor of ferroptosis restored the viability of *ABHD12*-deficient cells, as determined in a colony formation assay (Figure 5G). The results show that ABHD12 can inhibit the ferroptosis of liver cancer cells and therefore enhance sorafenib resistance.

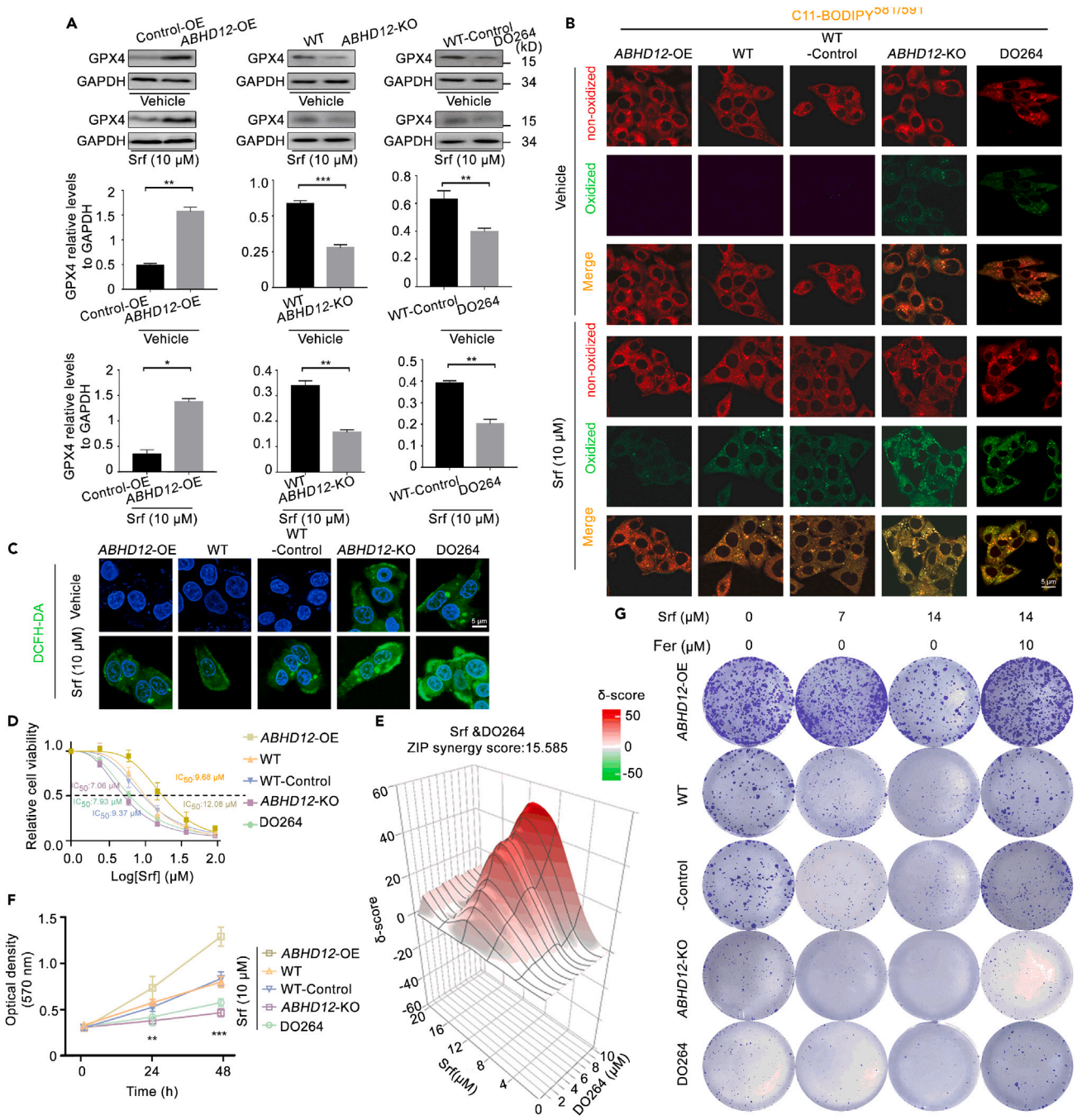

Figure 5. ABHD12 inhibits sorafenib-induced ferroptosis in HepG2 cells

Different HepG2 cell lines were used in the following experiments: Control-OE, cells treated with empty viral vector; WT, wild-type cells; *ABHD12-OE*, cells overexpressing *ABHD12*; WT-Control, wild-type cells treated with vehicle; *ABHD12-KO*, cells from which *ABHD12* was deleted; DO264, cells treated with ABHD12 inhibitor (DO264). Cells were treated with or without 10 μM sorafenib (Srf) for 24 h.

(A) The upper panel shows western blot analysis of GPX4 protein; the lower panel shows the corresponding densitometry. GAPDH was used as an internal control. Data are presented as mean ± SD (n = 3 independent experiments). *p < 0.05, **p < 0.01, ***p < 0.001.

(B) Confocal images of lipid reactive oxygen species (ROS), as detected by the fluorescent probe C11-BODIPY$^{581/591}$. Scale bar, 5 μm.

(C) Representative confocal images of intracellular ROS levels using the fluorescent probe DCFH-DA. Scale bar, 5 μm.

(D) IC_{50} values for sorafenib against different cell populations. Results are from three independent experiments.

(E) Surface plots for higher order drug combinations. Sorafenib and DO264 act synergistically on HepG2 cells. Sorafenib and DO264 at the indicated concentrations were used to treat cells for 24 h, and cell viability was assessed by MTT assay. ZIP Synergy scores were calculated using Synergyfinder

Figure 5. *Continued*

software. Scores > 0 indicated synergism, and scores > 10 were considered strong synergistic. The gradation of the red regions indicates the intensity of synergism. Results are from three independent experiments.

(F) Quantification of cell viability as assessed by MTT assay.

(G) Representative images of colony formation assay after cells were treated for 2 weeks with sorafenib at 0, 7, or 14 μM in the presence or absence of l0 μM ferrostatin-1 (Fer-1). Results are from three independent experiments. Abbreviations: OE, overexpressing; WT, wild-type; KO, knock out; Srf, sorafenib; ROS, reactive oxygen species; Fer-1, ferrostatin-1; GAPDH, glyceraldehyde-3-phosphate dehydrogenase; GPX4, antioxidant enzyme glutathione peroxidase 4.

ABHD12 inhibitor combined with sorafenib shows therapeutic efficacy against LIHC *in vivo*

Five HepG2 cells lines modified to express various levels of *ABHD12* were subcutaneously injected into nude mice (Figure 6A), and after tumors had reached a predefined size, mice were given oral sorafenib, DO264, or vehicle daily.[38] Mice whose tumors overexpressed *ABHD12* showed rapid tumor growth even in the presence of sorafenib, indicating sorafenib resistance. Conversely, mice whose tumors lacked *ABHD12* and mice treated with ABHD12 inhibitor showed sluggish tumor growth and smaller tumor masses in the presence of sorafenib, indicating sensitivity to the drug (Figures 6B–6E). Furthermore, GPX4 expression were detected in tumor by western blot after treatments; regardless of sorafenib treatment, pharmacological or genetic disruption of ABHD12 downregulated GPX4 in tumor (Figure 6F).

These results lead us to propose that ABHD12 contributes to tumorigenesis by promoting cell proliferation and migration as well as enhances sorafenib resistance by upregulating GPX4 to inhibit sorafenib-induced ferroptosis (Figure 6G). This implies that blocking *ABHD12* to induce ferroptosis may potentiate the activity of sorafenib against LIHC.

DISCUSSION

The already high incidence of LIHC continues to increase globally, together with the high rate of associated mortality.[39] Most patients are diagnosed when LIHC is at an advanced stage, which reduces their possibility to receive curative treatment. Sorafenib is a first-line treatment for advanced LIHC, but it can lead to drug resistance and ultimately to poor prognosis.[13] Therefore, future efforts to improve LIHC treatment should explore better screening measures for early detection of liver cancer and comprehensively elucidate on the mechanisms underlying sorafenib resistance to identify the biological alterations that are associated with an optimal efficacy of sorafenib, which may improve the accuracy of diagnosis and curative efficacy of chemotherapy. Here, we found that *ABHD12* is upregulated in LIHC and that it contributes to poor prognosis. We also showed that *ABHD12* contributes to proliferation and migration of liver cancer cells, inhibits ferroptosis, and enhances sorafenib resistance in LIHC, making it a promising target in the accurate diagnosis and treatment of LIHC patients. To our knowledge, this is the first report to comprehensively investigate the gene expression, function, and regulatory mechanism of *ABHD12* in LIHC by integrating data from bioinformatics, cell culture, patient biopsies, and a nude mouse tumor model.

Aberrant lipid metabolism has been linked to cancers and to disorders affecting the immune system, central nervous system, and metabolism. Cancer cells reprogram lipid metabolism to ensure a steady supply of energy and nutrients to promote proliferation and progression.[40] The α/β-hydrolase-domain-containing enzymes (ABHDs) play a role in lipid synthesis and degradation, and changes in lipid metabolism involve changes in expression of the *ABHD* gene family.[41,42] Indeed, members of the *ABHD* gene family are often differentially expressed in cancers. For example, ABHD12 is a lysophospholipase that can hydrolyze endocannabinoid 2-arachidonoylglycerol.[25] The endocannabinoid system can inhibit breast cancer,[28,43] and knockdown of *ABHD12* inhibits breast cancer cell growth, proliferation, migration, and invasion.[30] We found similar effects in our study when we genetically or pharmacologically knocked down *ABHD12* in HepG2 liver cancer cells. Similarly, *ABHD12* positively correlated with colorectal cancer based on analysis of copy-number aberration and gene expression.[44] In our study, TCGA data revealed that *ABHD12* was upregulated in LIHC patient tissue, which we confirmed in patient samples, and upregulation correlated with poor prognosis. Moreover, *ABHD12* expression positively correlated with that of genes regulating cell cycle, whereas a negative regulatory relationship with mismatch repair as well as GPX4 expression in TCGA data. We also confirmed that ABHD12 contributes to proliferation and migration of liver cancer cells *in vitro*. This study indicates the promising potential of *ABHD12* in the diagnosis and prognosis of liver cancer.

Cancer cells depend more on iron than normal cells do, making them more susceptible to ferroptosis.[45] As dysregulation of ferroptosis has been linked to chemoresistance,[46] it is crucial to explore why triggering ferroptosis can sensitize cancer cells to chemotherapy. Inducing ferroptosis may be a promising strategy for enhancing the sensitivity of sorafenib to tumor cells. For example, haloperidol, an antagonist of the Sigma-1 receptor, promotes sorafenib-induced ferroptosis death by increasing ROS accumulation.[47] Silencing metallothionein-1G sensitizes tumor cells to sorafenib in LIHC by triggering ferroptosis.[48] P62-KEAP1-NRF2 pathway inhibition enhanced the anticancer activity of sorafenib by inducing ferroptosis significantly *in vitro* and *in vivo* of LIHC.[49] GPX4 is considered a crucial targeting for triggering ferroptosis currently.[50] Here, we found that loss of *ABHD12* increased lipid peroxidation production, intracellular ROS levels, and subsequent ferroptosis. It also sensitized HepG2 cells to sorafenib by facilitating ferroptosis *in vitro*, whereas *ABHD12* overexpression had the opposite effects. The results of the present study are consistent with reports in fibrosarcoma cells that blockade of ABHD12 potentiates ferroptosis.[31]

ABHD12 has been shown to have a neutral lipase activity that acts on monoacylglycerols (MAGs), including 2-arachidonoyl glycerol (2-AG), pharmacological or genetic disruption of ABHD12 elevating 2-AG.[31] Moreover, 2-AG activates AMP-activated kinase (AMPK),[51] which promotes the nuclear accumulation of NRF2.[52] NRF2 is an essential transcription factor in maintaining cellular redox balance, which can activate the downstream antioxidant genes expression such as GPX4 by binding the antioxidant response element (ARE).[53,54] Therefore, ABHD12 may play a role in GPX4-dependent ferroptosis via the 2-AG-induced AMPK/NRF2/GPX4 axis. Besides, 2-AG is an

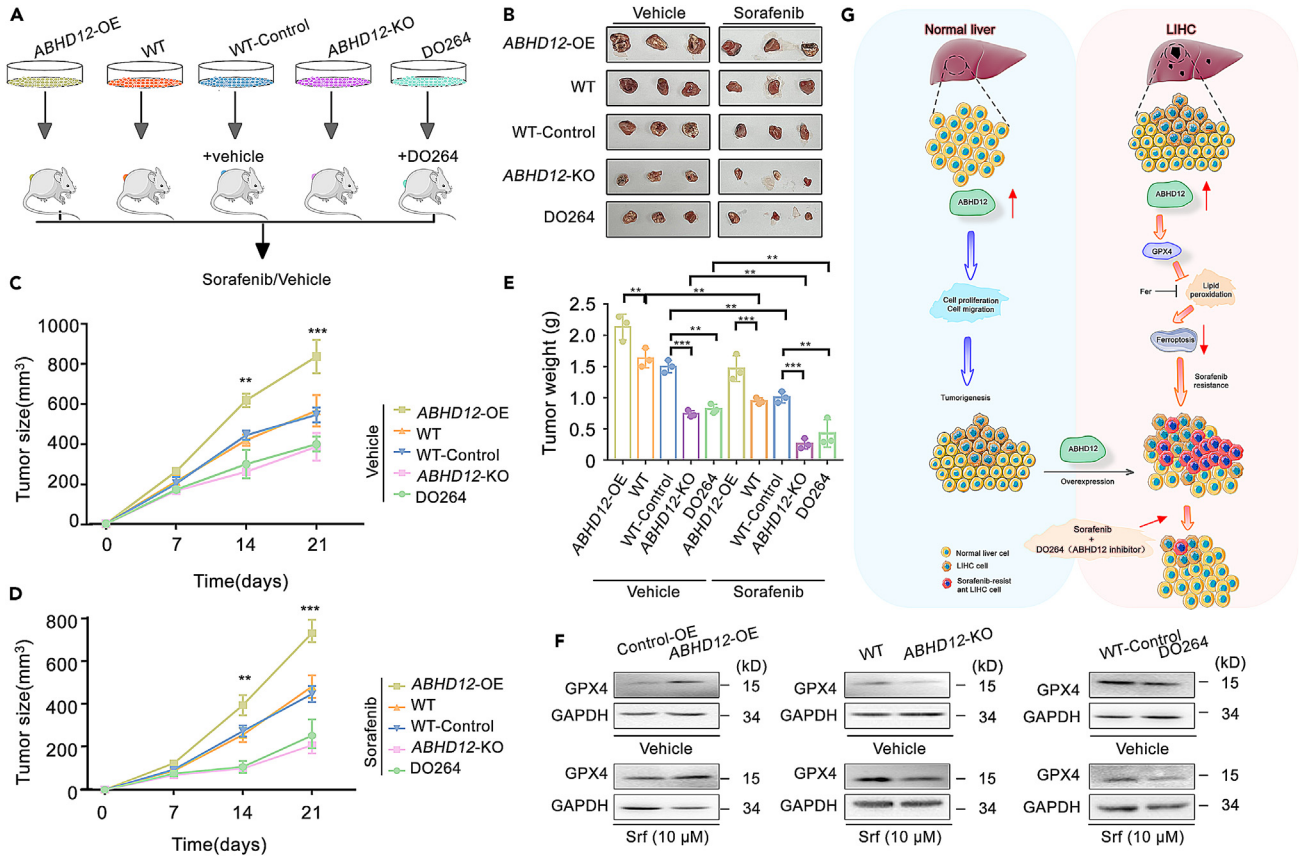

Figure 6. ABHD12 contributes to tumorigenesis and sorafenib resistance in liver cancer cells

(A) Schematic of the experimental design. Five HepG2 cells lines were used in the following experiments: WT, wild-type cells; *ABHD12-OE*, cells overexpressing *ABHD12*; WT-Control, cells treated with vehicle; *ABHD12-KO*, cells from which *ABHD12* was deleted; DO264, cells treated with ABHD12 inhibitor (DO264). Cells were implanted into nude mice, which were then treated with 20 mg/kg sorafenib (Srf), 30 mg/kg DO264, or DMSO vehicle.

(B) Photographs of tumor weights at sacrifice.

(C and D) Tumor sizes were measured once a week.

(E) Tumor weight. Data are shown as mean ± SD. Statistical significance was calculated using two-way ANOVA. **p < 0.01, ***p < 0.001.

(F) Western blot analysis of GPX4 protein in tumor. GAPDH was used as an internal control.

(G) A model for how *ABHD12* may contribute to tumorigenesis and sorafenib resistance of HepG2 cells. Abbreviations: OE, overexpressing; WT, wild-type; KO, knock out; LIHC, liver hepatocellular carcinoma; Fer, ferrostatin-1; GPX4, antioxidant enzyme glutathione peroxidase 4.

arachidonic acid (AA) derivative, sharing a 19-carbon backbone structure, that can diffuse across the cell membrane.[55] Studies show that in the cell culture medium that lacks AA, supplementation of exogenous AA may activate AMPK and enhance ferroptosis.[56] This may help to explain how the increased extracellular lipids make contribution to ferroptosis. In addition, protein-protein interaction networks predicted that ABHD12 may play a role in GPX4-dependent ferroptosis via another axis (Figures S6). ABHD12 interacts with NCEH1, a Neutral Cholesterol Ester Hydrolase,[57] as well as NDUFS1, which has NADH dehydrogenase activity and redox enzyme activity and affects the formation of reactive oxygen species (ROS).[58] Excessive accumulation of ROS can activate oxidative stress and may affect the activity of the antioxidant glutathione reductase (GSR). GSR plays an important role in maintaining intracellular redox balance by redoxing oxidized glutathione (GSSG) to GSH and the activity of GPX4 is directly affected by the synthesis and consumption of GSH.[59] Taken together, the two ways may help us to infer how ABHD12 regulates GPX4. Nevertheless, mechanism that ABHD12 inhibits ferroptosis needs further study. In addition, studies have shown that ABHD12-disrupted mice display heightened immune responses and ABHD12 inhibitor can promote immune function *in vivo*,[38] which may help explain why combining sorafenib with the ABHD12 inhibitor DO264 led to better anti-tumor efficacy than sorafenib alone in our animal study *in vivo*. Collectively, our findings suggest that ferroptosis plays an important role in the anti-tumor efficacy of sorafenib and that inhibition of ferroptosis may be a major mechanism of sorafenib resistance; ABHD12 plays a negative regulatory role in ferroptosis during sorafenib treatment; co-delivery of sorafenib and ABHD12 inhibitor into a nude mouse model of LIHC limited tumor growth more than sorafenib alone; and combination therapy involving sorafenib and an ABHD12 inhibitor was potential for the therapy of LIHC. The biological alterations of ABHD12 are associated with efficacy of sorafenib, which may help to personalize its use in LIHC.

To our best knowledge, this is the first study to explore the role of ABHD12 in LIHC. ABHD12 expression was upregulated in LIHC tissue, which correlated with poor prognosis. ABHD12 induces sorafenib resistance by preventing ferroptosis as well as exhibits pro-tumorigenic properties. Sorafenib together with ABHD12 inhibitor limited tumor growth more than sorafenib alone both *in vitro and in vivo*. In the context of sorafenib resistance as a major clinical challenge in the therapy of LIHC, we report first pre-clinical proof that ABHD12 inhibition together with sorafenib may offer attractive opportunities to overcome sorafenib and potentially other therapy resistance.

Limitations of the study

Through validation by large-scale samples from public databases, we identified a total of 7,687 differentially expressed genes (DEGs) between LIHC patients and normal controls from the TCGA database; preliminarily ABHD12 was consistently the most upregulated ABHD gene in LIHC. However, the number of samples used for immunohistochemistry analysis is small. We investigated associations between ABHD12 expression and clinicopathological characteristics with clinical samples of only 58 patients. The discovered molecular changes may also vary at different levels in different populations due to differences in race or region. To indicate that ABHD12 may be a potential diagnostic and prognostic biomarker for liver cancer still required more samples.

Our findings in Figure 5 suggest that ABHD12 inhibits sorafenib-induced ferroptosis and blockade of ABHD12 potentiates ferroptosis, whereas inducing ferroptosis may prevent the emergence of sorafenib resistance. However, our study does not prove how ABHD12 upregulates GPX4. As such, additional studies that investigate the interplay between ABHD12 biologically and GPX4 will help provide additional context to the molecular mechanism that ABHD12 promote ferroptosis resistance.

STAR★METHODS

Detailed methods are provided in the online version of this paper and include the following:

- KEY RESOURCES TABLE
- RESOURCE AVAILABILITY
  - Lead contact
  - Materials availability
  - Data and code availability
- EXPERIMENTAL MODEL AND STUDY PARTICIPANT DETAILS
  - Clinical samples
  - Tumor xenografts
- METHOD DETAILS
  - Plasmid constructs and gRNA design
  - Cell culture and transfection
  - Lentivirus generation and infection
  - Analysis of the TCGA database
  - Construction of a protein-protein interaction (PPI) network involving ABHD12
  - Kaplan Meier analysis of *ABHD* genes
  - Immunohistochemistry and liver cancer tissue microarrays
  - Real-time and semi-quantitative RT-PCR
  - Western blot analysis
  - Lipid peroxidation assay
  - ROS assay
  - Cell proliferation assays
  - Cell migration assays
  - Colony formation assay
  - Drug synergistic analysis
- QUANTIFICATION AND STATISTICAL ANALYSIS
- ADDITIONAL RESOURCES

SUPPLEMENTAL INFORMATION

Supplemental information can be found online at https://doi.org/10.1016/j.isci.2023.108340.

ACKNOWLEDGMENTS

The authors acknowledge financial support from the National Natural Science Foundation of China (82101687), the China National Key Research and Development (R&D) Program (2021YFC2100100), the China Postdoctoral Science Foundation (2021M690951), and the National Natural Science Foundation of China (82003688).

AUTHOR CONTRIBUTIONS

C.Y.B. and M.L.X.: Design of the study, resources, data curation, formal analysis, investigation, visualization, and drafting of the manuscript. C.M.X.: Experimental work and drafting of the manuscript. Y.X.P.: Experimental work. L.J.W. and Z.C.: Data analysis, visualization, and drafting of the manuscript. Y.C.X.: Provision of patient samples. C.Y.B.: Bioinformatic analysis and editing of the manuscript. All authors read and approved the final manuscript.

DECLARATION OF INTERESTS

The authors declare that they have no competing interests.

INCLUSION AND DIVERSITY

We support inclusive, diverse, and equitable conduct of research.

Received: June 29, 2023
Revised: October 5, 2023
Accepted: October 23, 2023
Published: October 27, 2023

REFERENCES

1. Aly, A., Ronnebaum, S., Patel, D., Doleh, Y., and Benavente, F. (2020). Epidemiologic, humanistic and economic burden of hepatocellular carcinoma in the USA: a systematic literature review. Hepat. Oncol. *7*, HEP27.
2. Rai, V., and Mukherjee, S. (2022). Targets of immunotherapy for hepatocellular carcinoma: An update. World J. Hepatol. *14*, 140–157.
3. Franses, J.W., and Zhu, A.X. (2022). Neoadjuvant Approaches in Hepatocellular Carcinoma: There's No Time Like the Present. Clin. Cancer Res. *28*, 2738–2743.
4. Fan, X., Wen, J., Bao, L., Gao, F., Li, Y., and He, D. (2021). Identification and Validation of DEPDC1B as an Independent Early Diagnostic and Prognostic Biomarker in Liver Hepatocellular Carcinoma. Front. Genet. *12*, 681809.
5. Villanueva, A. (2019). Hepatocellular Carcinoma. N. Engl. J. Med. *380*, 1450–1462.
6. Lu, F., Shah, P.A., Rao, A., Gifford-Hollingsworth, C., Chen, A., Trey, G., Soryal, M., Talat, A., Aslam, A., Nasir, B., et al. (2020). Liver Cancer-Specific Serine Protease Inhibitor Kazal Is a Potentially Novel Biomarker for the Early Detection of Hepatocellular Carcinoma. Clin. Transl. Gastroenterol. *11*, e00271.
7. Yang, J.D., Hainaut, P., Gores, G.J., Amadou, A., Plymoth, A., and Roberts, L.R. (2019). A global view of hepatocellular carcinoma: trends, risk, prevention and management. Nat. Rev. Gastroenterol. Hepatol. *16*, 589–604.
8. Wang, Q., Bin, C., Xue, Q., Gao, Q., Huang, A., Wang, K., and Tang, N. (2021). GSTZ1 sensitizes hepatocellular carcinoma cells to sorafenib-induced ferroptosis via inhibition of NRF2/GPX4 axis. Cell Death Dis. *12*, 426.
9. Louandre, C., Marcq, I., Bouhlal, H., Lachaier, E., Godin, C., Saidak, Z., François, C., Chatelain, D., Debuysscher, V., Barbare, J.C., et al. (2015). The retinoblastoma (Rb) protein regulates ferroptosis induced by sorafenib in human hepatocellular carcinoma cells. Cancer Lett. *356*, 971–977.
10. Cheng, A.L., Kang, Y.K., Chen, Z., Tsao, C.J., Qin, S., Kim, J.S., Luo, R., Feng, J., Ye, S., Yang, T.S., et al. (2009). Efficacy and safety of sorafenib in patients in the Asia-Pacific region with advanced hepatocellular carcinoma: a phase III randomised, double-blind, placebo-controlled trial. Lancet Oncol. *10*, 25–34.
11. Shuen, T.W.H., Alunni-Fabbroni, M., Öcal, E., Malfertheiner, P., Wildgruber, M., Schinner, R., Pech, M., Benckert, J., Sangro, B., Kuhl, C., et al. (2022). Extracellular Vesicles May Predict Response to Radioembolization and Sorafenib Treatment in Advanced Hepatocellular Carcinoma: An Exploratory Analysis from the SORAMIC Trial. Clin. Cancer Res. *28*, 3890–3901.
12. Verset, G., Borbath, I., Karwal, M., Verslype, C., Van Vlierberghe, H., Kardosh, A., Zagonel, V., Stal, P., Sarker, D., Palmer, D.H., et al. (2022). Pembrolizumab Monotherapy for Previously Untreated Advanced Hepatocellular Carcinoma: Data from the Open-Label, Phase II KEYNOTE-224 Trial. Clin. Cancer Res. *28*, 2547–2554.
13. Llovet, J.M., Montal, R., Sia, D., and Finn, R.S. (2018). Molecular therapies and precision medicine for hepatocellular carcinoma. Nat. Rev. Clin. Oncol. *15*, 599–616.
14. Raoul, J.L., Kudo, M., Finn, R.S., Edeline, J., Reig, M., and Galle, P.R. (2018). Systemic therapy for intermediate and advanced hepatocellular carcinoma: Sorafenib and beyond. Cancer Treat Rev. *68*, 16–24.
15. Lu, Y., Chan, Y.T., Tan, H.Y., Zhang, C., Guo, W., Xu, Y., Sharma, R., Chen, Z.S., Zheng, Y.C., Wang, N., and Feng, Y. (2022). Epigenetic regulation of ferroptosis via ETS1/miR-23a-3p/ACSL4 axis mediates sorafenib resistance in human hepatocellular carcinoma. J. Exp. Clin. Cancer Res. *41*, 3.
16. He, Y., Wang, X., Lu, W., Zhang, D., Huang, L., Luo, Y., Xiong, L., Li, H., Zhang, P., Li, Q., and Liang, S. (2022). PGK1 contributes to tumorigenesis and sorafenib resistance of renal clear cell carcinoma via activating CXCR4/ERK signaling pathway and accelerating glycolysis. Cell Death Dis. *13*, 118.
17. Dixon, S.J., Lemberg, K.M., Lamprecht, M.R., Skouta, R., Zaitsev, E.M., Gleason, C.E., Patel, D.N., Bauer, A.J., Cantley, A.M., Yang, W.S., et al. (2012). Ferroptosis: an iron-dependent form of nonapoptotic cell death. Cell *149*, 1060–1072.
18. Chen, X., Li, J., Kang, R., Klionsky, D.J., and Tang, D. (2021). Ferroptosis: machinery and regulation. Autophagy *17*, 2054–2081.
19. Zhang, Z., Yao, Z., Wang, L., Ding, H., Shao, J., Chen, A., Zhang, F., and Zheng, S. (2018). Activation of ferritinophagy is required for the RNA-binding protein ELAVL1/HuR to regulate ferroptosis in hepatic stellate cells. Autophagy *14*, 2083–2103.
20. Yang, W.S., SriRamaratnam, R., Welsch, M.E., Shimada, K., Skouta, R., Viswanathan, V.S., Cheah, J.H., Clemons, P.A., Shamji, A.F., Clish, C.B., et al. (2014). Regulation of ferroptotic cancer cell death by GPX4. Cell *156*, 317–331.
21. Gao, R., Kalathur, R.K.R., Coto-Llerena, M., Ercan, C., Buechel, D., Shuang, S., Piscuoglio, S., Dill, M.T., Camargo, F.D., Christofori, G., and Tang, F. (2021). YAP/TAZ and ATF4 drive resistance to Sorafenib in hepatocellular carcinoma by preventing ferroptosis. EMBO Mol. Med. *13*, e14351.
22. Nie, J., Lin, B., Zhou, M., Wu, L., and Zheng, T. (2018). Role of ferroptosis in hepatocellular carcinoma. Cancer Res. Clin. Oncol. *144*, 2329–2337.
23. Lachaier, E., Louandre, C., Godin, C., Saidak, Z., Baert, M., Diouf, M., Chauffert, B., and Galmiche, A. (2014). Sorafenib induces ferroptosis in human cancer cell lines originating from different solid tumors. Anticancer Res. *34*, 6417–6422.
24. Louandre, C., Ezzoukhry, Z., Godin, C., Barbare, J.C., Mazière, J.C., Chauffert, B., and Galmiche, A. (2013). Iron-dependent cell death of hepatocellular carcinoma cells exposed to sorafenib. Int. J. Cancer *133*, 1732–1742.
25. Blankman, J.L., Simon, G.M., and Cravatt, B.F. (2007). A comprehensive profile of brain enzymes that hydrolyze the endocannabinoid 2-arachidonoylglycerol. Chem. Biol. *14*, 1347–1356.
26. Pisanti, S., Picardi, P., D'Alessandro, A., Laezza, C., and Bifulco, M. (2013). The endocannabinoid signaling system in cancer. Trends Pharmacol. Sci. *34*, 273–282.
27. Laezza, C., Pisanti, S., Crescenzi, E., and Bifulco, M. (2006). Anandamide inhibits Cdk2 and activates Chk1 leading to cell cycle arrest

in human breast cancer cells. FEBS Lett. *580*, 6076–6082.
28. Cianchi, F., Papucci, L., Schiavone, N., Lulli, M., Magnelli, L., Vinci, M.C., Messerini, L., Manera, C., Ronconi, E., Romagnani, P., et al. (2008). Cannabinoid receptor activation induces apoptosis through tumor necrosis factor alpha-mediated ceramide de novo synthesis in colon cancer cells. Clin. Cancer Res. *14*, 7691–7700.
29. Kisková, T., Mungenast, F., Suváková, M., Jäger, W., and Thalhammer, T. (2019). Future Aspects for Cannabinoids in Breast Cancer Therapy. Int. J. Mol. Sci. *20*, 1673.
30. Jun, S., Kim, S.W., Lim, J.Y., and Park, S.J. (2020). ABHD12 Knockdown Suppresses Breast Cancer Cell Proliferation, Migration and Invasion. Anticancer Res. *40*, 2601–2611.
31. Kathman, S.G., Boshart, J., Jing, H., and Cravatt, B.F. (2020). Blockade of the Lysophosphatidylserine Lipase ABHD12 Potentiates Ferroptosis in Cancer Cells. ACS Chem. Biol. *15*, 871–877.
32. Chambers, J.C., Zhang, W., Sehmi, J., Li, X., Wass, M.N., Van der Harst, P., Holm, H., Sanna, S., Kavousi, M., Baumeister, S.E., et al. (2011). Genome-wide association study identifies loci influencing concentrations of liver enzymes in plasma. Nat. Genet. *43*, 1131–1138.
33. Xu, J., Gu, W., Ji, K., Xu, Z., Zhu, H., and Zheng, W. (2018). Sequence analysis and structure prediction of ABHD16A and the roles of the ABHD family members in human disease. Open Biol. *8*, 180017.
34. Li, P., Lin, Q., Sun, S., Yang, N., Xia, Y., Cao, S., Zhang, W., Li, Q., Guo, H., Zhu, M., et al. (2022). Inhibition of cannabinoid receptor type 1 sensitizes triple-negative breast cancer cells to ferroptosis via regulating fatty acid metabolism. Cell Death Dis. *13*, 808.
35. Mei, H., Zhao, L., Li, W., Zheng, Z., Tang, D., Lu, X., and He, Y. (2020). Inhibition of ferroptosis protects House Ear Institute-Organ of Corti 1 cells and cochlear hair cells from cisplatin-induced ototoxicity. J. Cell Mol. Med. *24*, 12065–12081.
36. Lin, M.T., and Beal, M.F. (2006). Mitochondrial dysfunction and oxidative stress in neurodegenerative diseases. Nature *443*, 787–795.
37. Chen, S., Zhu, J.Y., Zang, X., and Zhai, Y.Z. (2021). The Emerging Role of Ferroptosis in Liver Diseases. Front. Cell Dev. Biol. *9*, 801365.
38. Ogasawara, D., Ichu, T.A., Vartabedian, V.F., Benthuysen, J., Jing, H., Reed, A., Ulanovskaya, O.A., Hulce, J.J., Roberts, A., Brown, S., et al. (2018). Selective blockade of the lyso-PS lipase ABHD12 stimulates immune responses in vivo. Nat. Chem. Biol. *14*, 1099–1108.
39. Venook, A.P., Papandreou, C., Furuse, J., and de Guevara, L.L. (2010). The incidence and epidemiology of hepatocellular carcinoma: a global and regional perspective. Oncol. *15* (*Suppl 4*), 5–13.
40. Santos, C.R., and Schulze, A. (2012). Lipid metabolism in cancer. FEBS J. *279*, 2610–2623.
41. Lord, C.C., Thomas, G., and Brown, J.M. (2013). Mammalian alpha beta hydrolase domain (ABHD) proteins: Lipid metabolizing enzymes at the interface of cell signaling and energy metabolism. Biochim. Biophys. Acta *1831*, 792–802.
42. Thomas, G., Brown, A.L., and Brown, J.M. (2014). In vivo metabolite profiling as a means to identify uncharacterized lipase function: recent success stories within the alpha beta hydrolase domain (ABHD) enzyme family. Biochim. Biophys. Acta *1841*, 1097–1101.
43. Grimaldi, C., Pisanti, S., Laezza, C., Malfitano, A.M., Santoro, A., Vitale, M., Caruso, M.G., Notarnicola, M., Iacuzzo, I., Portella, G., et al. (2006). Anandamide inhibits adhesion and migration of breast cancer cells. Exp. Cell Res. *312*, 363–373.
44. Yoshida, T., Kobayashi, T., Itoda, M., Muto, T., Miyaguchi, K., Mogushi, K., Shoji, S., Shimokawa, K., Iida, S., Uetake, H., et al. (2010). Clinical omics analysis of colorectal cancer incorporating copy number aberrations and gene expression data. Cancer Inf. *9*, 147–161.
45. Torti, S.V., and Torti, F.M. (2013). Iron and cancer: more ore to be mined. Nat. Rev. Cancer *13*, 342–355.
46. Friedmann Angeli, J.P., Krysko, D.V., and Conrad, M. (2019). Ferroptosis at the crossroads of cancer-acquired drug resistance and immune evasion. Nat. Rev. Cancer *19*, 405–414.
47. Bai, T., Wang, S., Zhao, Y., Zhu, R., Wang, W., and Sun, Y. (2017). Haloperidol, a sigma receptor 1 antagonist, promotes ferroptosis in hepatocellular carcinoma cells. Biochem. Biophys. Res. Commun. *491*, 919–925.
48. Sun, X., Niu, X., Chen, R., He, W., Chen, D., Kang, R., and Tang, D. (2016). Metallothionein-1G facilitates sorafenib resistance through inhibition of ferroptosis. Hepatology *64*, 488–500.
49. Sun, X., Ou, Z., Chen, R., Niu, X., Chen, D., Kang, R., and Tang, D. (2016). Activation of the p62-Keap1-NRF2 pathway protects against ferroptosis in hepatocellular carcinoma cells. Hepatology *63*, 173–184.
50. Forcina, G.C., and Dixon, S.J. (2019). GPX4 at the Crossroads of Lipid Homeostasis and Ferroptosis. Proteomics *19*, e1800311.
51. Chanda, D., Oligschlaeger, Y., Geraets, I., Liu, Y., Zhu, X., Li, J., Nabben, M., Coumans, W., Luiken, J.J.F.P., Glatz, J.F.C., and Neumann, D. (2017). 2-Arachidonoylglycerol ameliorates inflammatory stress-induced insulin resistance in cardiomyocytes. J. Biol. Chem. *292*, 7105–7114.
52. Zhang, Y., Wu, Q., Liu, J., Zhang, Z., Ma, X., Zhang, Y., Zhu, J., Thring, R.W., Wu, M., Gao, Y., and Tong, H. (2022). Sulforaphane alleviates high fat diet-induced insulin resistance via AMPK/Nrf2/GPx4 axis. Biomed. Pharmacother. *152*, 113273.
53. Lu, Q., Yang, L., Xiao, J.J., Liu, Q., Ni, L., Hu, J.W., Yu, H., Wu, X., and Zhang, B.F. (2023). Empagliflozin attenuates the renal tubular ferroptosis in diabetic kidney disease through AMPK/NRF2 pathway. Free Radic. Biol. Med. *195*, 89–102.
54. Han, L., Yang, Q., Ma, W., Li, J., Qu, L., and Wang, M. (2018). Protocatechuic Acid Ameliorated Palmitic-Acid-Induced Oxidative Damage in Endothelial Cells through Activating Endogenous Antioxidant Enzymes via an Adenosine-Monophosphate-Activated-Protein-Kinase-Dependent Pathway. J. Agric. Food Chem. *66*, 10400–10409.
55. Kind, L., and Kursula, P. (2019). Structural properties and role of the endocannabinoid lipases ABHD6 and ABHD12 in lipid signalling and disease. Amino Acids *51*, 151–174.
56. Kong, P., Yang, M., Wang, Y., Yu, K.N., Wu, L., and Han, W. (2023). Ferroptosis triggered by STAT1- IRF1-ACSL4 pathway was involved in radiation-induced intestinal injury. Redox Biol. *66*, 102857.
57. Chang, J.W., Bhuiyan, M., Tsai, H.M., Zhang, H.J., Li, G., Fathi, S., McCutcheon, D.C., Leoni, L., Freifelder, R., Chen, C.T., and Moellering, R.E. (2020). In Vivo Imaging of the Tumor-Associated Enzyme NCEH1 with a Covalent PET Probe. Angew. Chem., Int. Ed. Engl. *59*, 15161–15165.
58. Qi, B., Song, L., Hu, L., Guo, D., Ren, G., Peng, T., Liu, M., Fang, Y., Li, C., Zhang, M., and Li, Y. (2022). Cardiac-specific overexpression of Ndufs1 ameliorates cardiac dysfunction after myocardial infarction by alleviating mitochondrial dysfunction and apoptosis. Exp. Mol. Med. *54*, 946–960.
59. Tang, D., Chen, X., Kang, R., and Kroemer, G. (2021). Ferroptosis: molecular mechanisms and health implications. Cell Res. *31*, 107–125.
60. Zhang, Y., Xu, X., Hu, M., Wang, X., Cheng, H., and Zhou, R. (2021). SPATA33 is an autophagy mediator for cargo selectivity in germline mitophagy. Cell Death Differ. *28*, 1076–1090.
61. Cheng, Y., Lai, F., Wang, X., Shang, D., Zou, J., Luo, M., Xia, X., Cheng, H., and Zhou, R. (2021). Srag Regulates Autophagy via Integrating into a Preexisting Autophagy Pathway in Testis. Mol. Biol. Evol. *38*, 128–141.
62. Bellio, P., Fagnani, L., Nazzicone, L., and Celenza, G. (2021). New and simplified method for drug combination studies by checkerboard assay. MethodsX *8*, 101543.
63. Segatore, B., Bellio, P., Setacci, D., Brisdelli, F., Piovano, M., Garbarino, J.A., Nicoletti, M., Amicosante, G., Perilli, M., and Celenza, G. (2012). In vitro interaction of usnic acid in combination with antimicrobial agents against methicillin-resistant Staphylococcus aureus clinical isolates determined by FICI and ΔE model methods. Phytomedicine *19*, 341–347.
64. Zhang, Q., Zhou, Y., Feng, X., Gao, Y., Huang, C., and Yao, X. (2022). Low-dose orlistat promotes the therapeutic effect of oxaliplatin in colorectal cancer. Biomed. Pharmacother. *153*, 113426.
65. Ianevski, A., Giri, A.K., and Aittokallio, T. (2020). SynergyFinder 2.0: visual analytics of multi-drug combination synergies. Nucleic Acids Res. *48*. W488–w493.
66. Zheng, S., Wang, W., Aldahdooh, J., Malyutina, A., Shadbahr, T., Tanoli, Z., Pessia, A., and Tang, J. (2022). SynergyFinder Plus: Toward Better Interpretation and Annotation of Drug Combination Screening Datasets. Dev. Reprod. Biol. *20*, 587–596.

STAR★METHODS

KEY RESOURCES TABLE

REAGENT or RESOURCE	SOURCE	IDENTIFIER
Antibodies		
ABHD12	Abcam	RRID: AB_182011
GPX4	Abcam	RRID: AB_125066
GAPDH	Abcam	RRID: AB_8245
Flag	Proteintech	RRID: AB_2749837
Bacterial and virus strains		
E. Coli strain DH5α	Tsingke	Cat# CTSC-C14
Biological samples		
Liver tumors and matched normal counterparts from liver cancer patients	Tongji Medical College	N/A
Chemicals, peptides, and recombinant proteins		
Sorafenib	Aladdin	Cat# S125098
Ferrostatin-1	Sigma	Cat# SML0583
DO264	MCE	Cat# 2301866-59-9
C11-BODIPY581/591	ThermoFisher	Cat# D3861
DCFH-DA	Yeasen	Cat# 50101ES01
Puromycin	Fisher Scientific	Cat# A1113802
Lipofectamine 3000 reagent	Invitrogen	Cat# 2233885
Critical commercial assays		
MTT	Invitrogen	Cat# M6494
BeyoClick™ EdU Cell Proliferation Kit with Alexa Fluor 647	Beyotime	Cat# C0081S
Peroxidase Conjugated Mouse/Rabbit IgG SP Kit	Solarbio	Cat# SP0041
FastKing gDNA Dispelling RT SuperMix	Tiangen	Cat# KR118
Deposited data		
Expression level of ABHD12 in LIHC tissues	TCGA Database	https://portal.gdc.cancer.gov/
Experimental models: Cell lines		
Hun7 cell	China Center for Type Culture Collection	N/A
HepG2 cell	China Center for Type Culture Collection	N/A
HEK293T cell	China Center for Type Culture Collection	N/A
Experimental models: Organisms/strains		
Nude mice	Hubei Animal Research Center	N/A
Oligonucleotides		
ABHD12-1-Bamh1: 5′-CGCGGATCCATGAGGAAGCGGACCGAG-3′	This paper	N/A
ABHD12-1-Xho1: 5′-CCGCTCGAGTCAGTGCTGGTGCTCAGG-3′	This paper	N/A
ABHD12-RTPCR-S: 5′ -TTCCAGCCACCCTATCAT-3′	This paper	N/A
ABHD12-RTPCR-A: 5′-AAACCCAGGGAAGTATCG-3′	This paper	N/A
ABHD12-crisper-S: 5′- CACCGGCGGACCGAGCCCGTCGCCT-3′	This paper	N/A

(*Continued on next page*)

Continued

REAGENT or RESOURCE	SOURCE	IDENTIFIER
ABHD12-crisper-A: 5′-AAACAGGCGACGGGCTCGGTCCGCC-3′	This paper	N/A
Recombinant DNA		
Plasmid: pMD2.G	Addgene	RRID: Addgene_12259
Plasmid: pRSV-Rev	Addgene	RRID: Addgene_ 12253
Plasmid: pCMV-VSV-G	Addgene	RRID: Addgene_ 8454
Plasmid: lentiCRISPRv2	Addgene	RRID: Addgene_52961
Plasmid: pSico-FLAG	BioVector	8627898
Software and algorithms		
ImageJ software	NIH	https://imagej.nih.gov/ij/
Graph-Pad Prism 8 version 8.3.0 software	GraphPad	https://www.graphpad.com/
R 3.6.0 software	R	https://www.r-project.org/
Online Oncolnc tool	Oncolnc	http://www.oncolnc.org/
Online GEPIA tool	GEPIA	http://gepia.cancer-pku.cn/

RESOURCE AVAILABILITY

Lead contact

Further information and requests for resources and reagents should be directed to and will be fulfilled by the lead contact, Yibin Cheng (chengyibin@hubu.edu.cn).

Materials availability

Plasmids and/or cell lines generated in this study are available upon reasonable request. Please contact the lead contact.

Data and code availability

- Expression level of ABHD12 in LIHC tissues data have been deposited at The Cancer Genome Atlas (TCGA) database https://portal.gdc.cancer.gov/.
- All data reported in this paper will be shared by the lead contact upon request.
- This paper does not report original code.
- Any additional information required to reanalyze the data reported in this paper is available from the lead contact upon request.

EXPERIMENTAL MODEL AND STUDY PARTICIPANT DETAILS

Clinical samples

Patients who underwent surgical resection for liver hepatocellular carcinoma were enrolled in our study. This study was approved by the Clinical Trial Committee of Huazhong University of Science and Technology (approval 2016L08026). Patients were fully informed of the aims and scope of the study and signed consent for their tissues to be used in this study. Patients were included in the study if they had a confirmed diagnosis of LIHC based on histopathological and radiological features and had complete clinical, pathological and laboratory data available. Patient information is listed in Table S2. Fresh tumor tissues and adjacent non-tumor tissues were obtained from 12 newly diagnosed liver cancer patients (10 males and 2 females, Chinese, Han) who underwent surgical resection. Tumor tissue arrays were prepared using a tissue array apparatus from 58 patients (55 males and 3 females, Chinese, Han) newly diagnosed with liver cancer who underwent surgical resection, from whom paraffin-embedded tumor tissues and adjacent nontumor tissues were also prepared. The gender of the patients did not have a significant influence on the study.

Tumor xenografts

4-week-old male BALB/c nude mice placed in five groups (n = 3) and implanted with one of the following HepG2 cell lines: Parental, wild-type cells; *ABHD12-OE*, cells overexpressing *ABHD12*; Parental-Control, wild-type cells treated with vehicle; *ABHD12-KO*, cells from which *ABHD12* was deleted; DO264, cells treated with ABHD12 inhibitor (DO264) (2301866-59-9, MCE, USA). Cells (each 6 × 10^7cells/mL in PBS*0.2 mL/mouse) were suspended in normal saline and were implanted into the left flanks of nude mice. When tumors were palpable, sorafenib (S125098; Aladdin, Shanghai, China) was applied at 20 mg/kg via gavage administered daily for 3 weeks, two groups of animals also received 30 mg/kg DO264 (2301866-59-9, MCE) during the same period. Tumor width and length were measured twice a week. Mice were

sacrificed after 3 weeks, and the tumors were collected. All animal experiments were approved by the Ethics Committee of the Wuhan Institute of Virology (approval WIVA04202102).

METHOD DETAILS

Plasmid constructs and gRNA design

The full-length human *ABHD12* sequence (NM_001042472.3) was cloned into pSico-FLAG using *Mfe*I and *Xho*I to generate pSico-FLAG-ABHD12. LentiCRISPRv2-*ABHD12*-gRNA was constructed as previously described.[60] Briefly, *ABHD12*-gRNAs were designed according to the CRISPR Design Tool (http://crispr.mit.edu/) and synthesized with a *Bsm*BI sticky end, subsequently, annealed and inserted into the lentiCRISPRv2 plasmid previously digested with *Bsm*BI (Fermentas, Vilnius, Lithuania). All primers are described in Table S4.

Cell culture and transfection

HEK293T and HepG2 cells were obtained from the China Center for Type Culture Collection and cultured in high-glucose Dulbecco's modified Eagle medium (catalog no. SH30022.01B, HyClone, Logan, USA) containing 10% fetal bovine serum (P30-330250, PAN-Biotech, Aidenbach, Germany) at 37°C in an environment containing 5% CO_2. For transfection, cells were cultured in cell plates or on glass coverslips according to the manufacturer's protocol, Lipofectamine 3000 (2233885, Invitrogen, Carlsbad, USA) was used in each well. Before analysis, the cells were cultured in sorafenib (catalog no. S125098, Aladdin, Shanghai, China), DO-264 (2301866-59-9, MCE, USA) or Ferrostatin-1 (SML0583, Sigma, USA) at the indicated times and concentrations.

Lentivirus generation and infection

To generate lentivirus as previously described,[4] HEK293T cells were transfected with lentiCRISPRv2-*ABHD12*-gRNA and lentiviral packaging vectors pMD2.G (12259, Addgene), pRSV-Rev (12253, Addgene, Watertown, USA), and pCMV-VSV-G (8454, Addgene) using Lipofectamine 3000 according to the manufacturer's instructions. After culture for 48 h, we use 0.45-μm filters to filter the supernatants then directly to infect HepG2 cells. After 24 h, we use the puromycin (A1113802, Fisher Scientific, Waltham, MA, USA) screen for transformants.

Analysis of the TCGA database

In our study, 371 LIHC tissues and 50 normal control tissues were obtained from The Cancer Genome Atlas (TCGA) database https://portal.gdc.cancer.gov/, then matched clinical parameters were extracted using the GDC Data Transfer Tool for secondary analysis. Using the corrplot program in R 3.6.0 software, we analyzed correlations between *ABHD* genes using Pearson's method. We use the limma package to look at the differences between LIHC tissues and normal controls in *ABHD* mRNA levels, which were quantified in terms of "fragments per kilobase of exon model per million mapped fragments" (FPKM). To visualize the findings, we used the pheatmap and ggpubr packages. Using data from 371 LIHC patients from the cBioPortal (http://www.cbioportal.org/), we examined patterns of somatic mutations, DNA copy-number alterations (CNAs), mRNA and microRNA (miRNA) expression, DNA methylation, protein abundance, and phosphorylated protein enrichment.

Construction of a protein-protein interaction (PPI) network involving ABHD12

PPI networks with ABHD12 were constructed using the Search Tool for the Retrieval of Interacting Genes (STRING) (https://string-db.org/).

Kaplan Meier analysis of *ABHD* genes

Overall survival (OS) of patients stratified by *ABHD* gene expression was performed using the online Oncolnc tool (http://www.oncolnc.org/). Disease-free survival (DFS) of patients stratified by *ABHD* gene expression was performed using the online GEPIA tool (http://gepia.cancer-pku.cn/). The log rank p value was calculated and analyzed, which identified *ABHD12* as having prognostic value.

Immunohistochemistry and liver cancer tissue microarrays

Tumor tissues and paired para-carcinoma tissues were paraffin-embedded, followed by dewaxing and blocking of endogenous peroxidase by 1% hydrogen peroxide. After incubation overnight at 4°C with anti-ABHD12 antibody (ab182011; Abcam, Cambridge, UK), tissue sections were washed, treated with biotinylated secondary antibody for 1 h at room temperature, reacted with 3,3- diaminobenzidine and counterstained with hematoxylin using the Peroxidase Conjugated Mouse/Rabbit IgG SP Kit (catalog no. SP0041; Solarbio, Beijing, China). The total score of protein expression was calculated by multiplying the percentage of immune-positive areas and immunostaining intensity.

Real-time and semi-quantitative RT-PCR

The total RNA was isolated by TRIzol (15596-026, Invitrogen, Carlsbad, CA, USA) from the clinical samples, then transcribed the RNA using FastKing gDNA Dispelling RT SuperMix (KR118, TIANGEN, China). Primer sequences are described in Table S4. Platinum SYBR Green qPCR Super Mix-UDG (D01010A, Invitrogen) was used for real-time PCR amplification of *ABHD12* in a real-time PCR system (Applied Biosystems, USA). *ACTIN* was used as an internal control.

Western blot analysis

Western blot analysis was performed as described.[61] Proteins were first extracted from HepG2 cells. Whole extracts were then analyzed by sodium dodecyl sulfate-polyacrylamide gel electrophoresis and transferred to a 0.45-μm polyvinylidene fluoride membrane (Roche Diagnostics, IN, USA). Membranes were blocked with 5% bovine serum albumin (BSA) in TBST (20 mM Tris-HCl, pH 7.5, 150 mM NaCl, 0.1% Tween 20), incubated with primary antibodies at 4°C overnight and then with the horseradish peroxidase-labeled secondary antibody. Proteins were detected using an enhanced chemiluminescence kit (Millipore, Billerica, MA, USA) and densitometry images were obtained using ImageJ software (vJ2, NIH, Maryland, US). Data were processed using Microsoft Excel.

Lipid peroxidation assay

Cells were seeded onto glass coverslips to visualize lipid ROS, treated as indicated, then stained with 10 μM C11-BODIPY$^{581/591}$ probe (ThermoFisher) in accordance to the manufacturer's instructions. After at 37°C with 5% CO_2 in the dark, then fixed the cell with 4% PFA for 20 min, washed with PBS, and stained with DAPI for 5 min. Subsequently, an LSM 980 confocal laser scanning microscope equipped with an oil immersion objective (Plan Apochromat 60× 1.40 NA), was used to collect optical sections every 1.5 μm to generate z-stacks. Each image represented the maximum projection of all slices along the z stack. Cells were analyzed from at least nine randomly selected regions of interest across three independent experiments. The fluorescence intensity was measured by ImageJ (National Institutes of Health).

ROS assay

Levels of intracellular ROS were evaluated based on uptake of DCFH-DA (50101ES01, Yeasen). HepG2 cells were seeded onto glass coverslips, treated under the indicated conditions, stained with 10 μM DCFH-DA for 30 min in the dark, then stained with Hoechst nuclear stain for 5 min. Images were acquired using an LSM 980 confocal laser scanning microscope equipped with an oil immersion objective (Plan Apochromat 60× 1.40 NA), and optical sections were collected every 1.5 μm to generate z-stacks. Each image represented the maximum projection of all slices along the z stack.

Cell proliferation assays

The MTT and EdU incorporation assays were used to measure cell proliferation. For MTT assays, cells were seeded in a 96-well plate at appropriate density per well. At the indicated times, 50 μL MTT solution was added to each well and incubated for another 4 h at 37°C in an environment containing 5% CO_2, 120 μL DMSO was added to each well then. The absorbance was measured at 570 nm of each well at various time points by the PerkinElmer 2030 Victor X multilabel plate reader (PerkinElmer).

For EdU incorporation assays, the BeyoClick™ EdU Cell Proliferation Kit with Alexa Fluor 647 (Beyotime) was used according to the manufacturer's protocol. Cells were observed using an LSM 980 confocal laser scanning microscope (Zeiss Microsystems), and images were analyzed using an IN-Cell Analyzer 2500HS imaging system (GE Healthcare Life Science, Chicago, IL, USA).

Cell migration assays

For transwell cell migration assays, equal amounts of cells were suspended in 100 μL of serum-fee medium and added to the upper chamber of 24-well transwell plates containing an 8.0-μm Pore Polycarbonate Membrane Insert (Corning Incorporated, Corning, NY, USA). The chamber insert was pre-warmed medium at 37°C with 100 μL of serum-free. Then 600 μL of complete medium was added to the lower chamber. After 24 h, removed the cells remaining in the upper chamber using cotton swabs, and washed the transwell inserts with PBS. Using 4% PFA (paraformaldehyde) to fixed the cells that migrated to the lower surface of the membrane and then stained with 0.1% crystal violet solution. Migrated cells were observed and counted under a microscope (IX73; OLYMPUS).

For wound healing migration assays, cells were seeded into 6-well plates. After the cells reached 80–90% confluence, using a sterile 10-μL pipette tip to wound the monolayer cell and washed with thrice PBS. In the presence of 4 μg/mL mitomycin (Roche) for the indicated times, cells were allowed to migrate while inhibit cell division. The wounds were visualized and imaged under a microscope (IX73; OLYMPUS). After wounding, the gap widths were imaged at 0 and 24 hours then measured from the micrographs. The changes of cell migration were determined by comparing the differences wound healing in at least 4 fields per slide using Image J (National Institutes of Health).

Colony formation assay

Cells were seeded into 12-well plates and cultured for 2 weeks with drug treatments; culture medium with drug treatments was exchanged every 24 h. After the culture period, cells were twice washed with PBS and fixed with 4% PFA for 20 min at room temperature, then washed with PBS again, stained with crystal violet for 40 min at room temperature. Washing with PBS again, after plates were left to dry, then the stained cells were quantified using Image J (National Institutes of Health).

Drug synergistic analysis

HepG2 cells were seeded into a 96-well plate at appropriate density per well and treated with different drug combinations by checkerboard assay.[62,63] After 24 h of treatment, by MTT assays, the optical density (OD) was measured. The online SynergyFinder software (https://synergyfinder.fimm.fi) was used to calculate drug synergy scoring with the "viability index" by the response surface model and zero interaction

potency (ZIP) calculation method.[64,65] ZIP Synergy scores greater than 0 were considered synergism (red regions), and scores greater than 10 were considered strong synergistic.[66]

QUANTIFICATION AND STATISTICAL ANALYSIS

Data were presented as mean ± standard deviation. Statistical comparisons were made using Student's *t* test when comparing two groups, or one-way analysis of variance (ANOVA) with Tukey's post hoc test when comparing more than two groups. Other statistical analyses were performed using SPSS 22. Differences with $p < 0.05$ were considered to be statistically significant. *, $p < 0.05$, **, $p < 0.01$, ***, $p < 0.001$.

ADDITIONAL RESOURCES

Clinical samples of this study were obtained from diagnosed liver cancer patients who underwent surgical resection, and the study protocol was approved by the ethics committee of Huazhong University of Science and Technology (approval 2016L08026).